Application of multi-pulse optical imaging to measure evolution of laser-produced counter-streaming flows*

Dawei Yuan(袁大伟)[1], Yutong Li(李玉同)[2,3,8,†], Baojun Zhu(朱保君)[2], Yanfei Li(李彦霏)[2], Jiayong Zhong(仲佳勇)[4,8], Huigang Wei(魏会冈)[1], Chang Liu(刘畅)[4], Xiaoxia Yuan(原晓霞)[4], Zhe Zhang(张喆)[2], Guiyun Liang(梁贵云)[1], Feilu Wang(王菲鹿)[1], Fang Li(李芳)[2], Jiarui Zhao(赵家瑞)[2], Neng Hua(华能)[5], Baoqiang Zhu(朱宝强)[5], Jianqiang Zhu(朱健强)[5], Shaoen Jiang(江少恩)[6], Kai Du(杜凯)[6], Yongkun Ding(丁永坤)[6], Gang Zhao(赵刚)[1,‡], and Jie Zhang(张杰)[7,8,§]

[1] *Key Laboratory of Optical Astronomy, National Astronomical Observatories, Chinese Academy of Sciences, Beijing* 100012, *China*
[2] *National Laboratory for Condensed Matter Physics, Institute of Physics, Chinese Academy of Sciences, Beijing* 100190, *China*
[3] *School of Physical Sciences, University of Chinese Academy of Sciences, Bejing* 100049, *China*
[4] *Department of Astronomy, Beijing Normal University, Beijing* 100875, *China*
[5] *National Laboratory on High Power Lasers and Physics, Shanghai* 201800, *China*
[6] *Research Center for Laser Fusion, China Academy of Engineering Physics, Mianyang* 621900, *China*
[7] *Key Laboratory for Laser Plasmas (Ministry of Education) and Department of Physics and Astronomy, Shanghai Jiao Tong University, Shanghai* 200240, *China*
[8] *Collaborative Innovation Center of IFSA (CICIFSA), Shanghai Jiaotong University, Shanghai* 200240, *China*

(Received 4 November 2016; revised manuscript received 6 December 2016; published online 30 March 2017)

A counter-streaming flow system is a test-bed to investigate the astrophysical collisionless shock (CS) formation in the laboratory. Electrostatic/electromagnetic instabilities, competitively growing in the system and exciting the CS formation, are sensitive to the flows parameters. One of the most important parameters is the velocity, determining what kind of instability contributes to the shock formation. Here we successfully measure the evolution of the counter-streaming flows within one shot using a multi-pulses imaging diagnostic technique. With the technique, the average velocity of the high-density-part ($n_e \geq 8$–9×10^{19} cm^{-3}) of the flow is directly measured to be of $\sim 10^6$ cm/s between 7 ns and 17 ns. Meanwhile, the average velocity of the low-density-part ($n_e \leq 2 \times 10^{19}$ cm^{-3}) can be estimated as $\sim 10^7$ cm/s. The experimental results show that a collisionless shock is formed during the low-density-part of the flow interacting with each other.

Keywords: collisionless shock, electrostatic/electromagnetic instabilities, imaging diagnostic technique

PACS: 42.30.−d, 47.80.Jk, 52.35.Tc, 52.35.Fp **DOI:** 10.1088/1674-1056/26/5/054206

1. Introduction

Astrophysical collisionless shock (CS) is common in many universal systems, such as supernova remnants (SNRs),[1,2] gamma-ray bursts (GRBs),[3,4] and protostellar jets. The counter-streaming flows system in absence of an external magnetic field is a well-scaled-down test-bed to investigate the CS formation in the laboratory. Recently, a series of simulation[5–11] and experiment results[12–18] have demonstrated that the self-generated electrostatic field/electromagnetic field growing in such an unmagnetized system can excite the CS generation. It is also found that the parameters of the plasma flow are crucial to these instabilities. For example, both flows with different properties (density, temperature) can enhance the shock formation process.[7] High density ($N_e > 10^{18}$ cm^{-3}) will easily generate shock because of the short ion inertia length (c/ω_{pi}).[18] High electron and ion temperature ($T_e > 1$ keV) will effectively reduce the field dissipation and the collision in the intra-stream.[18] High flow velocity (V) determines not only the collisionless mechanism of CS, but also the growth rate (γ) of the instabilities. For the Weibel instability, the growth rate can be expressed as[16,17] $\gamma \sim (0.2$–$0.5)V/\lambda$, where V is the flow velocity and λ is the ion inertia length. Only when the velocity is high enough to satisfy the condition of the growth rate being much larger than the dissipation rate, can the magnetic field grow up and excite shock formation.

Here we focus on the measurement of the flow velocity. Traditionally, the flow velocity can be obtained by the following methods. One is utilizing the streaked interferogram and self-emission optical pyrometry (SOP) taken in the same shot. Using this method, we can only measure the velocity at the specific position of the target, which is determined by the slit at the front of the streak camera. The other one is measuring

*Project supported by the National Basic Research Program of China (Grant No. 2013 CBA01501/3), the National Natural Science Foundation of China (Grant Nos. 11503041, 11135012, 11375262, 11573040, 11574390, and 11220101002), and China Postdoctoral Science Foundation (Grant No. 2015M571124).

†Corresponding author. E-mail: ytli@iphy.ac.cn
‡Corresponding author. E-mail: gzhao@bao.ac.cn
§Corresponding author. E-mail: jzhang1@sjtu.edu.cn

the velocity over different separate shots by changing the delay time between the probe beam and the driven beam.[12,13,15–19] Although we can obtain the lateral distribution of the flow velocity, the error is uncertain; it is because the laser conditions cannot be perfectly repeated.

In this paper, a multi-pulse imaging method is applied to measure the flow velocity in a single shot. The experimental data show that the velocity of the high-density-part of the flow before interaction can be directly measured using our new technique. The velocity of the low-density-part of the flow can be estimated under the quasi-isothermal free expansion assumption. In addition, the data also demonstrate that an isolated shock excited by the low-density-part interacting with each other is observed, which is similar to that observed in our previous experiment.[13,19] The paper is organized as follows. In Section 2, the experimental setup is described and the probe beam working models are given. Section 3 presents the experimental results and the corresponding discussion. The conclusion is presented in Section 4.

2. Experimental setup

The experiment was performed at the Shenguang II (SG-II) laser facility, which can output a 1 ns laser pulse of total energy 2 kJ at the wavelength of 351 nm. The eight driven laser beams were divided into two bunches and each bunch then consisted of four beams. Figure 1 shows a schematic diagram of the experimental setup, which is similar to that in our previous work.[13,19–24] A pair of opposing copper (Cu) foils were separated by 4.5 mm. One bunch was focused on the left-foil (in the end view) with a spot diameter of 150 μm. While the other one was defocused on the right-foil (in the end view) with a larger diameter of 300 μm. The counter-streaming flows were generated under such asymmetric ablation conditions.

The interaction between the counter-streaming flows was measured by the optical diagnostics, including Nomarski interferometry and shadowgraphy. A laser beam with a wavelength of 527 nm, transverse to the propagation of the flows, was used as a probe. The magnification of the imaging system was about 2.6–2.7, which was achieved by a two-stage imaging system. In order to obtain the same magnification for different optical paths, both imaging lenses were placed in front of the beam splitter (BS),[25] as shown in the top view of Fig. 1. Two charge coupled devices (CCD) recorded the same magnification images from both paths. In addition, the gate width of the CCD was set at 2 ns to keep data acquisition at the same conditions.

For comparison, the evolution of the counter-streaming flows was measured by two methods. Figure 2 shows the probe beam working models, i.e., single-pulse model and multi-pulse model. For the single-pulse model in Fig. 2(a), there was only one pulse with the duration of 30 ps. For the multi-pulse model in Fig. 2(b), there were two main pulses with a constant time separation of 10 ns. The first pulse duration was 30 ps; and the second pulse duration was about 1.2 ns, consisting of 4 single-pulses.

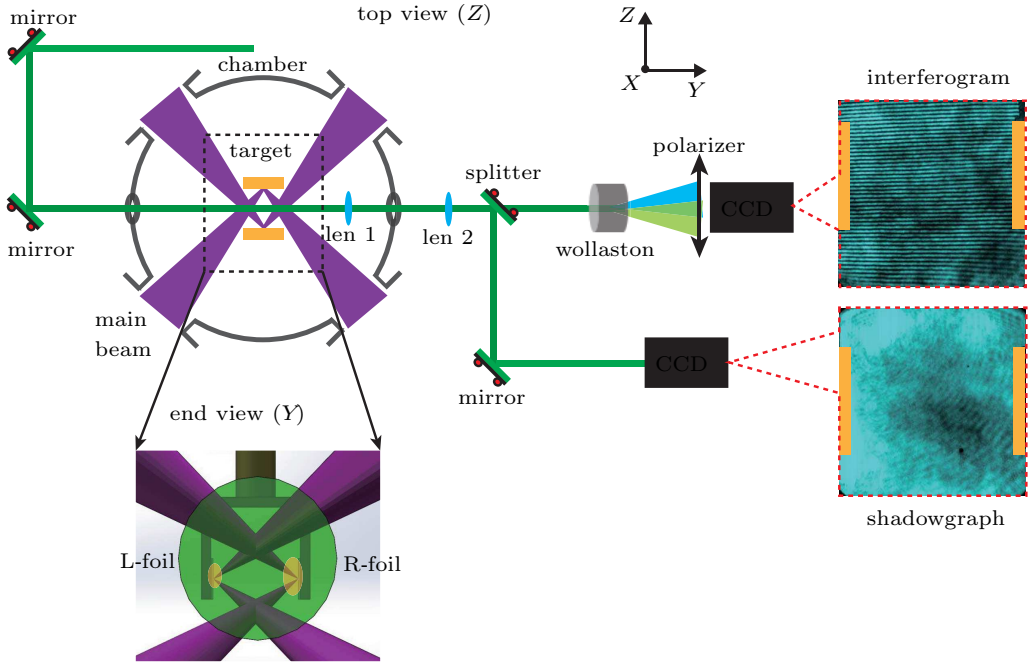

Fig. 1. (color online) Schematic view of experimental setup. Main laser beams divided into two bunches heated on the facing surfaces of the target to generate counter-streaming flows. The interaction of the two counter-streaming flows was measured by Nomarski interferometry and shadowgraphy. A 527 nm, 30 ps laser beam passing through the interaction region was used as a probe beam, which was split into two beams by a beam splitter after passing through the second imaging lens. One was for Nomarski interferometry to obtain the electron density, and the other was for shadowgraphy, which is sensitive to the second derivative of the electron density.[7] The inset images are the original ones before shooting. Two yellow regions on both sides stand for the initial position of the target.

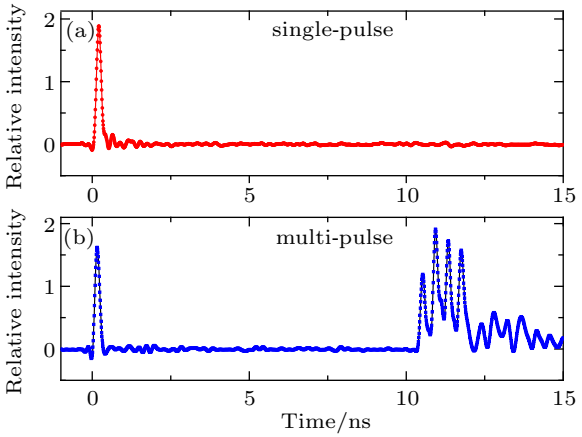

Fig. 2. (color online) The laser pulse of the probe beam. (a) The probe beam working at single-pulse model with duration of 30 ps. (b) The probe beam working at multi-pulse model. There are two main pulses, which are separated by 10 ns. The first main pulse duration is 30 ps; the second main pulse consists of 4 single pulses, whose duration is about 1.2 ns.

3. Experimental results and discussion

Figure 3 shows the counter-streaming flows obtained by the probe beams working at different models. A static reference image before shooting is displayed in Fig. 3(a). Two yellow columns on both sides represent the initial positions of the target foils. The gray circle represents the field of view, which is determined by an aperture with a diameter of 4.5 mm in front of the CCD. Figures 3(b) and 3(c) show the images obtained by the probe beam working at single-pulse model at T_0+7 ns and T_0+17 ns (the corresponding delay times are 7 ns and 17 ns, as shown in Figs. 3(e) and 3(f)), respectively. Here $T = T_0$ is the arrival time of the driven laser pulses at the target surface. At 7 ns, two dark bubble regions appear on both sides and a bright region in the middle area. The dark bubble represents the high plasma density region and the probe beam cannot pass through it (high-density-part). The bright region represents that the forepart of the plasma flow has a low plasma density and the probe beam can pass through it (low-density-part). At 17 ns, the dark bubbles on both sides continue expanding and an isolated dark quasi-plane appears in the middle area. Figure 3(d) is an overlapped image obtained by the probe beam working at the multi-pulse model (as shown in Fig. 3(g)). There are two components: one is the darker bubble region on both sides marked by the white dotted line, which is similar to that appearing at 7 ns in Fig. 3(b), the other one is a less dark expansion region on both sides and an isolated quasi-plane appears in the middle area, which is similar to that appearing at 17 ns as shown in Fig. 3(c). In order to accurately identify the difference between Figs. 3(c) and 3(d), we plot the probe intensity profiles along the target normal direction at the different transverse positions, which are marked by the different colors lines.

Figure 4 shows the corresponding probe intensity profiles of Figs. 3(b) and 3(c). The intensity suddenly changes in the middle area, which indicates that a large density jump exits

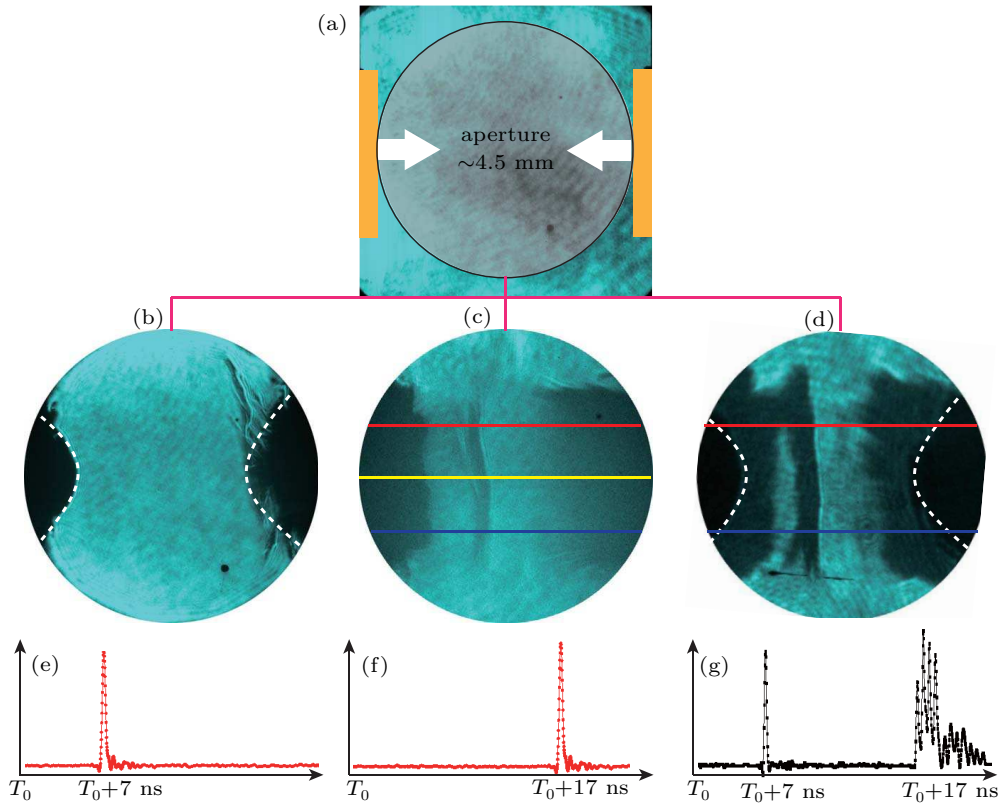

Fig. 3. (color online) The evolution of the counter-streaming flows obtained at different working models of the probe beam. (a) A static reference image before shooting. (b)–(d) The evolution of the counter-streaming flows obtained by different methods. (e)–(g) The working models of the probe beam.

and a shock is formed.[12] The width of the shock in Fig. 3(b) is about 200 μm and its position is at around 1.640 μm (±0.060 μm), as shown in Figs. 4(a)–4(c). The width of the shockwave in Fig. 3(c) is about 400 μm and its position is at around 1.490 μm (±0.090 μm), as shown in Figs. 4(d)–4(f). Although there are a few differences existing between the two measurements, their shapes are similar to a quasi-plane (laminar). In addition, the properties of the isolated shock indicate that the shock results from the low-density-part (foreparts) of both flows, not from the high-density-part (dark bubble) of the flows. The ion–ion mean free path (MFP) is an important parameter to determine whether the shock is collisionless. The MFP expression is given as $\lambda_{ii}=m_i^2 v_{rel}^4/\left(4\pi e^4 \bar{Z}^3 N_e \mathrm{Ln}\Lambda_{12}\right)$, where $m_i=Am_p$ is the ion mass, e is the electric charge, $\bar{Z}=10$ is the average ionization state, $n_e \sim 10^{19}$ cm^{-3} is the electron density of each flow (discussed below), and $\mathrm{Ln}\Lambda_{12} \approx 10$ is the Coulomb logarithm. The relative velocity between the two flows v_{rel} is larger than $2v_{flow}=5\times10^7$ cm/s (discussed below). Taking these values into the above expression, the MFP is obtained as $\sim$ 11 mm, much larger than the shock width ($\sim$ 200–400 μm). This indicates that the observed shock in the experiment is collisionless. Its formation and evolution are under investigation and will be described in our future publication.[26]

Figure 5 shows the lateral average velocity distribution of the dark bubble obtained by the muti-pulse method. From the measurement, the velocity of the high-density-part is on the order of $\sim$ (5–8) $\times$ 10^6 cm/s, which is directly obtained by the different positions of the sharp edge at different delay times. Obviously, the velocity on both sides is larger than that in the central region; it is probably caused by the thermal energy transverse transmission (temperature gradient) along the foil surface after the laser. As for the low-density-part of the flow, the velocity can be estimated under the assumption that the flow can be regard as a quasi-isothermal free expansion in the later time.[27] The evolution of each flow is predicated to have density $n \approx n_{ab}\exp(-\alpha x/C_s t)+\Delta N$ and flow velocity $V \approx C_s + x/t$. Here C_s is the sound speed, x measures the distance from the target, and t is time. The ablation density n_{ab} is on the order of the critical density, and α is a factor of order 1.

Figure 6(a) shows the distributions of the electron density and the flow velocity along the target normal direction (Y) at the central axis (labeled by the white dotted-line in Fig. 5). The electron density n_e along the Y direction is obtained by the Abel inversion of the interferograms. One can find that

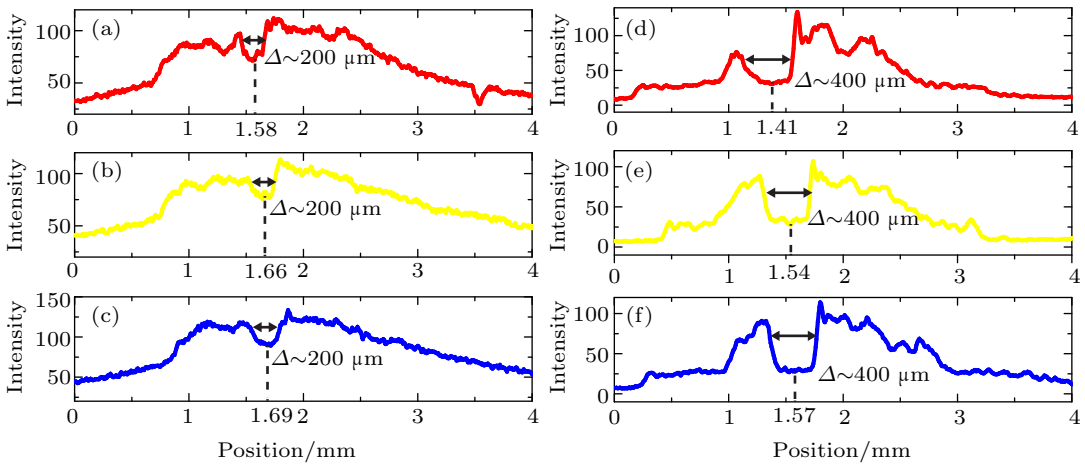

Fig. 4. (color online) The average intensity profiles corresponding to (a)–(c) Fig. 3(b) and (d)–(f) Fig. 3(c). The colors of the different curves correspond to the different positions in Fig. 3.

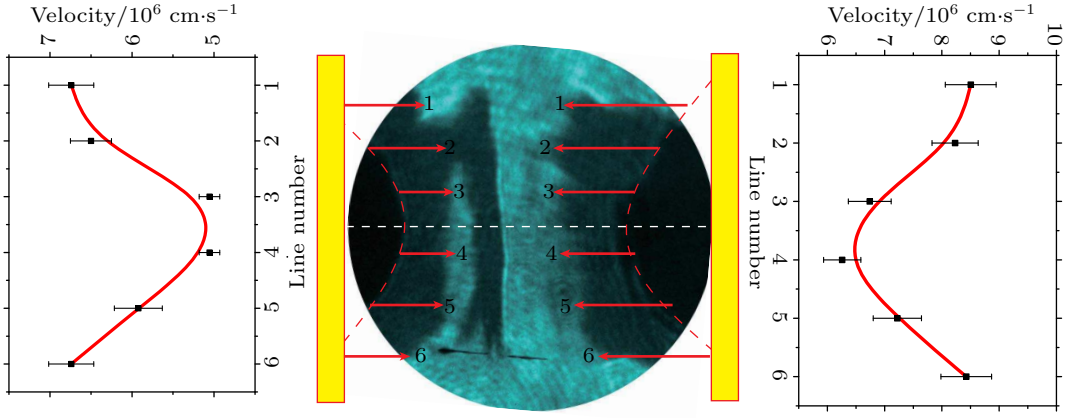

Fig. 5. (color online) The velocity distribution along the target surface on both sides obtained by the novel method.

the electron density of the high-density-part is above (8–9) × 10^{19} cm^{-3}, and the electron density of the low-density-part is below 2×10^{19} cm^{-3}. Using the above formula, the flow velocity of the low-density-part is estimated to be on order of $\sim 10^7$ cm/s, which is increasing with the dropping electron density.

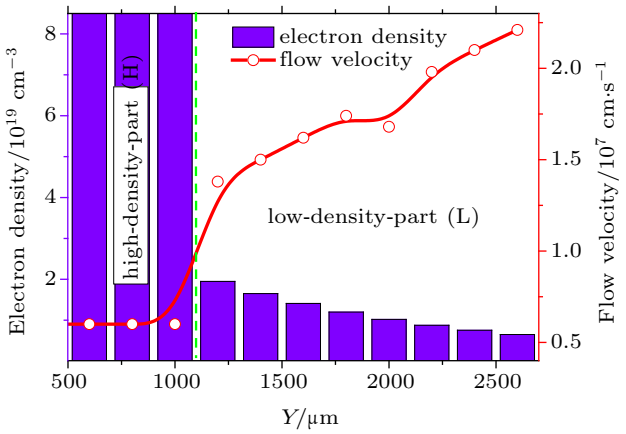

Fig. 6. (color online) The distributions of electron density and flow velocity at the central axis between 7 ns and 17 ns.

For application of the novel multi-pulse imaging diagnostic technique, two factors should be considered. (i) In order to distinguish the changes of the propagation distance of the flow at the different delay time, the distance change within 10 ns should be larger than the space resolution of the diagnostics, that is, $\overline{V}_{\rm flow} \times 10$ ns ≥ 50 μm (here the resolution is determined by CCD and the imaging system). Typically, the flow velocity generated at the large-energy (kJ-level) and long-duration (ns-level) laser facility, such as SG-II, Gekko-XII, OMEGA, etc. is on the order of $\sim 10^7$–10^8 cm/s. The propagation distance can be estimated as $\overline{V}_{\rm flow} \times 10$ ns $= 10^3 - 10^4$ μm, much larger than the resolution limit. Therefore, the technique can be applied in such laser-plasma experiments. If the flow velocity is below 10^6 cm/s, the technique can also be applied by shortening the time separation between the pulses or improving the resolution of the diagnostic. (ii) The second pulse of the probe beam consists of 4 individual pulses (the whole duration is about 1.2 ns). Within the second pulse, the distance changes can be estimated as (5–8) $\times 10^6$ cm/s $\times$ 1.2 ns = (60–100) μm, which is comparable to the resolution (50 μm). It means that the system cannot resolve the changes within the second pulses. Therefore, it is reasonable to ignore the effect on the quality of imaging. The probe can be approximately regarded as only containing two pulses, i.e., the first pulse with a duration of 30 ps and the second pulse with a duration of 1.2 ns.

4. Conclusion

We apply a multi-pulse method to measure the evolution of the counter-streaming flows. The average velocity of the denser part of the flow is directly measured to be $\sim$ (5–9) $\times 10^6$ cm/s within 7–17 ns, whose value depends on the transverse position. The low dense part of the flow is estimated to have a velocity on the order of 10^7 cm/s under the quasi-isothermal free expansion assumption. By comparing our new method with the traditional method, one can see that the experimental results can be well repeated. It indicates that using the new method can enhance the credibility of the experiment data. Additionally, this new method is flexible and can be widely applied in the laser-plasma experiment by optimizing the technical parameters, such as the time separation between the pulses and the resolution of the diagnostic.

Acknowledgement

The authors thank the staff of the SG-II laser facility for operating the laser and target area.

References

[1] Bamba A, Yamazaki R, Ueno M and Koyama K 2003 *Astrophys. J.* **589** 827
[2] Uchiyama Y, Aharonian F A, Tanaka T, Takahashi T and Maeda Y 2007 *Nature* **449** 576
[3] Medvedev M V, Silva L O, Fiore M, Fonseca R A and Mori W B 2004 *J. Korean Astron. Soc.* **37** 533
[4] Remington B A, Drake R P and Ryutov D D 2006 *Rev. Mod. Phys.* **78** 755
[5] Forslund D W and Shonk C R 1970 *Phys. Rev. Lett.* **25** 1699
[6] Kato T N and Takabe H 2010 *Phys. Plasmas* **17** 032114
[7] Sorasio G, Marti M, Fonseca R and Silva L O 2006 *Phys. Rev. Lett.* **96** 045005
[8] Sarri G, Dieckmann M E, Kourakis I and Borghesi M 2011 *Phys. Rev. Lett.* **107** 025003
[9] Ruyer C, Gremillet L and Bonnaud G 2015 *Phys. Plasmas* **22** 082107
[10] Fiuza F, Fonseca R A, Tonge J, Mori W B and Silva L O 2012 *Phys. Rev. Lett.* **108** 235004
[11] Stockem A, Fiuza F, Bret A, Fonseca R A and Silva L O 2014 *Scientific Reports* **4** 3934
[12] Morita T, Sakawa Y, Kuramitsu Y, Dono S, Aoki H, Tanji H, Kato T N, Li Y T, Zhang Y, Liu X, Zhong J Y, Takabe H and Zhang J 2010 *Phys. Plasmas* **17** 122702
[13] Liu X, Li Y T, Zhang Y, Zhong J Y, *et al.* 2011 *New J. Phys.* **13** 093001
[14] Kuramitsu Y, Sakawa Y, Morita T, Gregory C D, Waugh J N, Dono S, Aoki H, Tanji H, Koenig M, Woolsey N and Takabe H 2011 *Phys. Rev. Lett.* **106** 175002
[15] Kugland N L, Ryutov D D and Chang P Y *et al.* 2012 *Nat. Phys.* **8** 809
[16] Fox W, Fiksel G, Bhattacharjee A, Chang P Y, Germaschewski K, Hu S X and Nilson P M 2013 *Phys. Rev. Lett.* **111** 225002
[17] Huntington C M, Fiuza F, Ross J S, *et al.* 2015 *Nat. Phys.* **11** 173
[18] Park H-S, Huntington C M, Fiuza F, *et al.* 2015 *Phys. Plasmas* **22** 056311
[19] Yuan D W, Li Y T, Liu X, Zhang Y, Zhong J Y, Zheng W D, Dong Q L, Chen M, Sakawa Y, Morita T, Kuramitsu Y, Kato T N, Takabe H, Rhee Yong-Joo, Zhu J Q, Zhao G and Zhang J 2013 *High Energy Density. Phys.* **9** 239
[20] Zhong J Y, Li Y T, Wang X G, Wang J Q, Dong Q L, Xiao C J, Wang S J, Liu X, Zhang L, An L, Wang F L, Zhu J Q, Gu Y, He X T, Zhao G and Zhang J 2010 *Nat. Phys.* **6** 984
[21] Dong Q L, Wang S J, Lu Q M, *et al.* 2012 *Phys. Rev. Lett.* **108** 215001
[22] Yuan D W, Wu J F, Li Y T, *et al.* 2015 *Astrophys. J.* **815** 46
[23] Wang F L, Pei X X, Han B, *et al.* 2016 *High Power Laser Science and Engineering* **4** e27
[24] Liao G Q, Li Y T, Zhu B J, *et al.* 2015 *Matter Radiat. Extrem.* **1** 187
[25] Buck A, Nicolai M, Schmid K, Sears C M S, Sävert A, Mikhailova J M, Krausz F, Kaluza M C and Veisz L 2011 *Nat. Phys.* **7** 543
[26] Yuan D W, *et al*, 2017 *Shock Formation and Evolution in the Asymmetry Laser-produced Counter-streaming Flows* (In preparation)
[27] Manheimer W M, Colombant D G and Gardner J H 1982 *Phys. Fluids* **25** 1644